TLR4 Inactivation in Myeloid Cells Accelerates Bone Healing of a Calvarial Defect Model in Mice

Dan Wang, D.M.D, Ph.D.
James R. Gilbert, Ph.D.
Gwen M. Taylor, Ph.D.
Chhinder P. Sodhi, Ph.D.
David J. Hackam, M.D, Ph.D.
Joseph E. Losee, M.D.
Timothy R. Billiar, M.D.
Gregory M. Cooper, Ph.D.

Shanghai, People's Republic of China; Pittsburgh, Pa.; and Baltimore, Md.

Background: Toll-like receptor 4 (TLR4) has been implicated in inflammation-induced bone destruction in various chronic bone diseases; however, its direct influence on bone healing is not well understood. The authors' previous study showed accelerated bone healing with higher osteoclastogenesis gene expression in toll-like receptor 4 knockout mice ($TLR4^{-/-}$). This study aimed to further elucidate the underlying cellular mechanisms during fracture healing by generating a myeloid cell-specific toll-like receptor 4 knockout model (Lyz-$TLR4^{-/-}$ mice).

Methods: Calvarial defects, 1.8 mm in diameter, were created in wild-type, $TLR4^{-/-}$, and Lyz-$TLR4^{-/-}$ mice. Bone healing was investigated using micro–computed tomography and histologic, histomorphometric, and immunohistochemistry analyses. Primary bone marrow–derived cells were also isolated from wild-type, $TLR4^{-/-}$, and Lyz-$TLR4^{-/-}$ mice to measure their osteoclast differentiation and resorption properties.

Results: A similar faster bone healing response, with active intramembranous bone formation, intense osteopontin staining, and more osteoblast infiltration, was observed in $TLR4^{-/-}$ and Lyz-$TLR4^{-/-}$ mice. Tartrate-resistant acid phosphatase staining showed more osteoclast infiltration in Lyz-$TLR4^{-/-}$ mice than in wild-type mice at day 7. Primary bone marrow–derived cells isolated from $TLR4^{-/-}$ and Lyz-$TLR4^{-/-}$ mice presented enhanced osteoclastogenesis and resorption activity compared with those from wild-type mice. Comparable M0, M1, and M2 macrophage infiltration was found among all groups at days 1, 4, and 7.

Conclusions: This study revealed that inactivation of toll-like receptor 4 in myeloid cells enhanced osteoclastogenesis and accelerated healing response during skull repair. Together with the role of toll-like receptor 4 in inflammation-mediated bone destruction, it suggests that toll-like receptor 4 might regulate inflammation-induced osteoclastogenesis under different clinical settings. (*Plast. Reconstr. Surg.* 140: 296e, 2017.)

Skeletal development and tissue regeneration use many similar molecular mechanisms, some of which lie dormant and activate only in response to injury. Inflammation, an integral component of the injury response, is involved not only in the host defense against infectious pathogens but also in tissue repair and regeneration, dynamically balancing its tissue-destructive and tissue-constructive properties.[1,2] For decades, osteoimmunology has focused mostly on investigating osteoclasts and metabolic

From the Department of Stomatology, Tenth People's Hospital of Tongji University; the Departments of Plastic Surgery, Surgery, Oral Biology, and Bioengineering, University of Pittsburgh; and the Department of Surgery, The Johns Hopkins University.

Received for publication September 20, 2016; accepted February 15, 2017.

Presented in part at the 2013 American Society for Bone and Mineral Research Annual Meeting, in Baltimore, Maryland, October 2016.

DOI: 10.1097/PRS.0000000000003541

Disclosure: *All authors have no financial interest to declare in relation to the content of this article.*

Supplemental digital content is available for this article. Direct URL citations appear in the text; simply type the URL address into any Web browser to access this content. Clickable links to the material are provided in the HTML text of this article on the *Journal*'s website (www.PRSJournal.com).

bone disease as they relate to pathologic bone resorption.[3] Recently, interest has increased in elucidating the positive interactions between the immune and skeletal systems during the fracture healing process.[4]

Toll-like receptors are a family of transmembrane receptors that activate the innate immune response by recognizing conserved molecular patterns of microbial products and endogenous ligands.[5] Toll-like receptor 4 (TLR4) signaling is of particular interest in regenerative biology because of its pronounced impact on healing in diverse models of injury and sterile inflammatory disease.[6,7] It can recognize a wide range of pathogen-associated molecular patterns and damage-associated molecular patterns, including bacterial lipopolysaccharide[8] and endogenous molecules such as fibrinogen,[9] fibronectin,[10] heat shock proteins 60 and 70,[11] β-Defensin 2,[12] and high-mobility group protein B1.[13]

Toll-like receptor 4 is expressed mainly in immune cells, such as monocytes/macrophages, dendritic cells, T cells and B cells, and bone cells such as osteoblasts and osteoclasts.[14] Although the expression of different toll-like receptors varies with different stages of osteoclast differentiation, expression of toll-like receptor 2 and toll-like receptor 4 has been reported within all osteoclast-lineage cells.[14] Thus, it is not surprising that toll-like receptor 4 is involved in inflammation-induced osteoclast differentiation and bone destruction in various chronic bone diseases, such as osteoarthritis and periodontitis.[15,16] In addition, toll-like receptor 4 polymorphism has also been shown to play a role in the etiopathogenesis of postmenopausal osteoporosis and periodontitis.[17,18] However, the direct influence of toll-like receptor 4 signaling components on fracture healing is not thoroughly understood.

In a previous study, we observed accelerated bone healing with higher RANKL (receptor activator of nuclear factor kappa-B ligand) expression in toll-like receptor 4 global knockout mice at day 4 after surgery (TLR4$^{-/-}$) in a noncompromised mouse calvarial defect model.[19] Because of the apparent correlation between increased osteoclastogenesis and improved bone healing, we hypothesized that the increased healing observed in TLR4$^{-/-}$ mice was attributable to the loss of toll-like receptor 4 signaling in osteoclast precursor cells. To test this hypothesis, we used a myeloid cell- specific TLR4$^{-/-}$ mouse model (TLR4$^{flox/-, lyz\ cre}$ or TLR4$^{loxp/-; Lyz\text{-}cre}$) to further elucidate the underlying cellular mechanisms during facture healing.

MATERIALS AND METHODS

Mouse Strains and Generation of Myeloid-Specific TLR4$^{-/-}$ Mice

Wild-type (C57BL-6J; The Jackson Laboratory, Bar Harbor, Me.), TLR4$^{-/-}$, and Lyz-TLR4$^{-/-}$ female mice between 10 and 16 weeks of age and weighing 20 to 30 g were used in this study. Lyz-TLR4$^{-/-}$ mice were developed by breeding TLR4$^{loxp/-; Lyz\text{-}cre}$ mice with TLR4$^{loxp/loxp}$ mice.[20,21] Tail snips of offspring were collected at 21 days of age for genotyping using polymerase chain reaction. As TLR4$^{-/-}$ mice are viable without baseline abnormalities, we anticipated no baseline phenotypic variation in the mice with toll-like receptor 4 deleted from specific cell types. All procedures were carried out in accordance with regulations regarding for the care and use of experimental animals published by the National Institutes of Health and approved by the University of Pittsburgh Institutional Animal Use and Care Committee.

Surgical Procedure

Wild-type, TLR4$^{-/-}$, and Lyz-TLR4$^{-/-}$ mice were anesthetized with isoflurane (4% by inhalation and 2% by duration), and 1.8-mm-diameter defects were created on mouse parietal bones as described previously.[19] Ketoprofen (Fort Dodge Animal Health, Fort Dodge, Iowa), 1 mg/kg, was administered as an analgesic immediately and for 2 days after surgery. All mice were killed by means of carbon dioxide overdose followed by cervical dislocation at designated time points.

Micro–Computed Tomographic Analyses

Wild-type, TLR4$^{-/-}$, and Lyz-TLR4$^{-/-}$ mice were killed at 0, 7, and 28 days after surgery. The skulls were dissected and stored in 4% paraformaldehyde overnight and later stored in 70% ethanol. The calvarial defect healing process was analyzed in three dimensions using a high-resolution micro–computed tomography system (Inveon microCT; Siemens, Erlangen, Germany) with a fixed isotropic voxel size of 15 μm. Three-dimensional images were reconstructed using Amira software (FEI Visualization Sciences Group, Burlington, Mass.) and OsiriX software. Quantitative data were analyzed by OsiriX software with a global fixed threshold −330 and a region of interest (4mm^2 × 2.09mm) was defined.[19] Standard micro–computed tomographic measurements (regenerated bone volume = bone volume within the region of interest at day 7, and 28 – bone volume at day 0) were calculated for each sample using OsiriX software.

Histology and Histomorphometric Analyses

Wild-type, TLR4$^{-/-}$, and Lyz-TLR4$^{-/-}$ mice were killed at day 0 and postoperative days 1, 4, 7, 14, and 28. Calvariae and surrounding soft tissues (e.g., skin, brain) were harvested and fixed in 4% paraformaldehyde for 24 hours. Samples were decalcified in 10% ethylenediaminetetraacetic acid before being dehydrated through a series of ethanol and embedded in paraffin.[19] Paraffin-embedded specimens were sectioned through the coronal plane at a thickness of 5 to 6 μm. Slides were stained with Harris' hematoxylin and eosin (Surgipath Medical Industries, Richmond, Ill.) for conventional, qualitative bright-field light microscopy.

Russell-Movat pentachrome staining (American MasterTech, Lodi, Calif.) was performed to further differentiate the following tissues within the defect: hematoma/fibrin (intense red), elastic fibers (black), newly formed woven bone (yellow), and lamellar bone (red). For tartrate-resistant acid phosphatase staining, sectioned slides were first incubated in phosphate-buffered saline (pH = 5) at 37°C for 5 minutes and then incubated in tartrate-resistant acid phosphatase buffer (pH = 5) containing 0.1 mol/liter acetate buffer, 0.3 mol/liter sodium tartrate, 10 mg/ml naphthol AS-MX phosphate (Sigma-Aldrich Corp., St. Louis, Mo.), 100 μl Triton X-100, and 0.3 mg/ml Fast Red Violet LB salt (Sigma-Aldrich) for 1 hour at 37°C. Sections were counterstained with 0.02% fast green (Sigma-Aldrich) before mounting in Cytoseal 280 (Fisher Scientific, Pittsburgh, Pa.). Osteoclasts were detected as tartrate-resistant acid phosphatase–positive cells.

Histomorphometric analyses were performed to quantify cellular infiltration and two-dimensional areas of new bone formation using a Leica MZ12 microscope (Leica Microsystems Ltd., Heerbrugg, Switzerland) and Northern Eclipse (v5.0) image analysis software (Empix, Imaging, Inc., Cheektowage, N.Y.). Bone healing data were calculated based on three to five slides per animal. New areas of bone formation were visually identified under 100× magnification. New bone area was calculated as the sum of the areas of each bone section, including within the defect and on both sides of the calvaria. The sum totals of newly formed bone areas were averaged by the numbers of slides per animal.[22] Osteoblasts were calculated as the total number of osteoblasts per osteoblast-lining bone surface under 100× magnification. Osteoclasts were calculated as the total number of osteoclasts per field under 200× magnification. Data were expressed as mean ± SEM. All measurements were performed in a blinded fashion.

Immunohistochemistry Analyses

Sections from wild-type, TLR4$^{-/-}$, and Lyz-TLR4$^{-/-}$ mice were deparaffinized with xylenes and rehydrated through a decreasing series of ethanol to distilled water. Antigen retrieval was performed on all samples using a Universal Antigen Retrieval Kit (R&D Systems, Minneapolis, Minn.). Following the manufacturer's instructions, sections were incubated in 10% blocking serum for 1 hour at room temperature. Sections were then incubated in primary antibodies, which were suspended in 10% blocking serum overnight at 4°C. Sections were incubated in horseradish peroxidase–conjugated secondary antibody (dilution, 1:250) for 30 minutes at room temperature. Color was developed by application of a *diaminobenzidine* kit (Vector Laboratories, Burlingame, Calif.). Horse and goat blocking serum came from Vector Laboratories. Primary antibodies were goat polyclonal anti-osteopontin (dilution, 1:250) as a marker of osteogenic differentiation, rabbit polyclonal anti-F4/80 (dilution 1:250) as a marker for M0 macrophages, rabbit polyclonal anti-CD163 (dilution, 1:250) as a marker for M1 macrophages, and goat polyclonal anti-arginase1 (dilution, 1:250) as a marker for M2 macrophages (Santa Cruz Biotechnology, Santa Cruz, Calif.; Abcam, Cambridge, Mass.). Secondary antibodies were anti-goat horse immunoglobulin G and anti-rabbit goat immunoglobulin G (Vector Laboratories). Sections were dehydrated and mounted before examination under 25×, 50×, 100×, 200×, and 400× magnifications.

In Vitro Bone Marrow–Derived Osteoclast Differentiation Assay

Femora and tibiae were excised from 9- to 10-week-old female mice (wild-type, TLR4$^{-/-}$, and Lyz-TLR4$^{-/-}$). The soft tissue and connective tissue were carefully removed and the ends of the bones were cut off. Bone marrow was flushed out using a 5-ml syringe into a 50-ml tube with Dulbecco's Modified Eagle Medium (Life Technology, Grand Island, N.Y.). Bone marrow suspension was centrifuged at 1000 rpm, 4°C, for 5 minutes. The supernatant was removed and the cells were suspended in the Dulbecco's Modified Eagle Medium media containing 10% fetal bovine serum, 1% penicillin/streptomycin, and 10 ng/ml macrophage colony-stimulating factor (Life Technologies, Carlsbad, Calif.). The cell suspension was seeded onto a 6-cm

diameter cell culture dish overnight. Unattached cells were collected and seeded with Dulbecco's Modified Eagle Medium containing 10% fetal bovine serum, 1% penicillin/streptomycin, and 30 ng/ml macrophage colony-stimulating factor at 10^4 cells/well on a 96-well plate (Corning Osteo Assay Surface; Corning, Tewksbury, Mass.). Three days after seeding, the medium was changed to fresh Dulbecco's Modified Eagle Medium containing 10% fetal bovine serum, 1% penicillin/streptomycin, 30 ng/ml macrophage colony-stimulating factor, and 50 ng/ml RANKL (Life Technologies).

For tartrate-resistant acid phosphatase staining and resorption assay, at days 8 and 11 after osteoclast differentiation culture, cells were fixed with 10% buffered paraformaldehyde solution. Fixed cells were stained with a tartrate-resistant acid phosphatase kit (Takaba, Clontech Laboratories, Calif.) according to the manufacturer's protocol. After staining, tartrate-resistant acid phosphatase–positive multinucleated cells were quantified under 100× magnification. The osteoclast ratio was calculated as the number of osteoclasts over the total number of cells per image. To perform resorption analysis, 10% bleach solution was added to lyse cells. After washing three times with phosphate-buffered saline, plates were air-dried at room temperature for 5 hours. Resorption pits were imaged under 100× magnification and Adobe Photoshop (Adobe Systems, Inc., San Jose, Calif.) was used for quantification analysis.

Statistical Analyses

Statistical analyses were performed using IBM SPSS Version 20.0 software (IBM Corp., Armonk, N.Y.). Data (i.e., mean bone volume calculation from micro–computed tomographic analyses, mean areas of newly formed bone, number of osteoblasts/bone surface and number of osteoclasts/bone area collected from histomorphometric measurements, and osteoclast ratio and areas of resorption pits from in vitro osteoclast differentiation analyses) were compared using one-way analysis of variance followed by the post hoc least significant difference test. A value of $p < 0.05$ was considered significant.

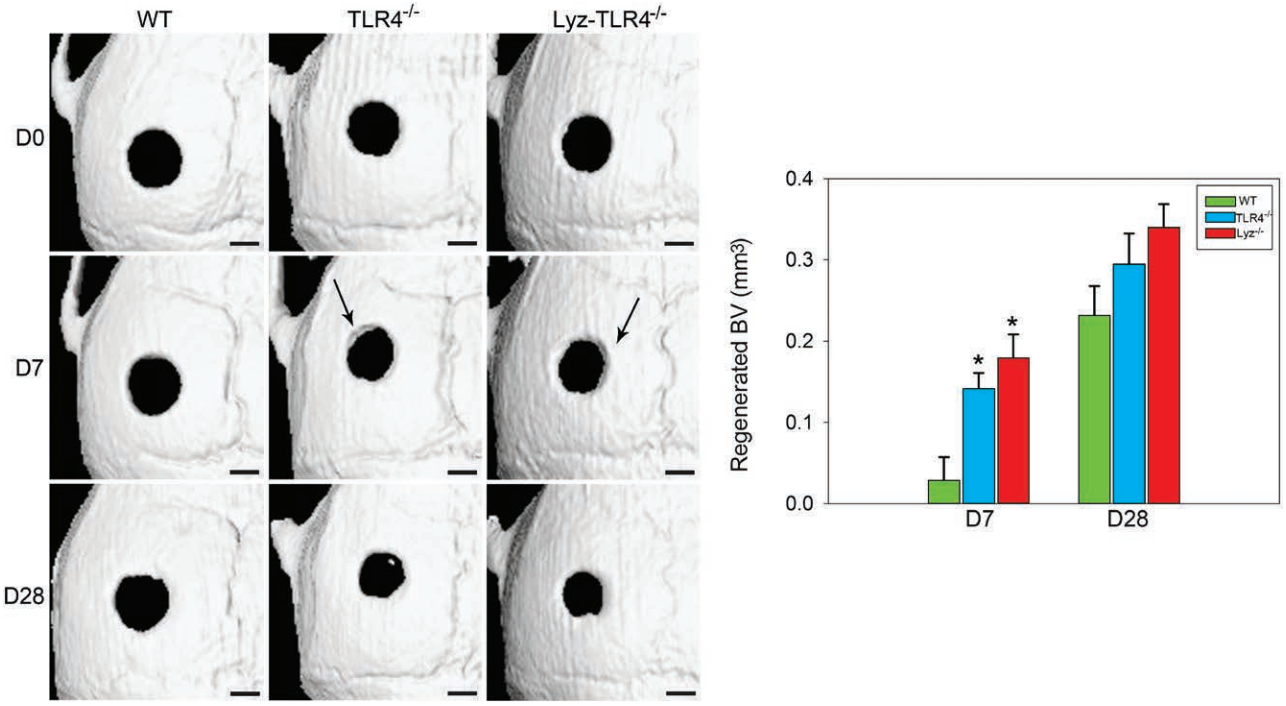

Fig. 1. Micro–computed tomographic analyses of calvarial defect healing at postoperative days 0, 7, and 28 of wild-type, TLR4$^{-/-}$, and Lyz-TLR4$^{-/-}$ mice. (*Left*) Representative three-dimensional reconstructions of calvarial defects in the transverse plane at different time points. Faster healing was evident in TLR4$^{-/-}$ and Lyz-TLR4$^{-/-}$ mice, as indicated by more mineralized tissue around the defect edges at day 7 (*arrows*). Similar bone healing was shown among the three groups on day 28. (*Right*) Bone volume (*BV*) measurements at different time points. Significantly larger bone volume was found in TLR4$^{-/-}$ and Lyz-TLR4$^{-/-}$ mice relative to wild-type mice at day 7, whereas no significant differences were seen between the three groups at day 28. No significant difference in bone volume between TLR4$^{-/-}$ and Lyz-TLR4$^{-/-}$ mice was seen at either days 7 or 28 ($n = 6$ to 8 mice per group per time point, mean ± SEM; *scale bar* = 500 μm; $p < 0.05$, *versus wild-type).

RESULTS

Accelerated Intramembranous Bone Formation in TLR4$^{-/-}$ and Lyz-TLR4$^{-/-}$ Mice

To characterize the bone healing process, micro–computed tomography was performed on three groups of mice (wild-type, TLR4$^{-/-}$, and Lyz-TLR4$^{-/-}$) at postoperative days 0, 7, and 28. Representative three-dimensional reconstructed images are shown in Figure 1. No group showed complete bone healing within 28 days of observation. At day 7, areas of mineralized tissue were observed in TLR4$^{-/-}$ and Lyz-TLR4$^{-/-}$ mice, whereas no obvious new bone formation was evident in wild-type mice (Fig. 1, *left*). Significantly larger bone volume was found in TLR4$^{-/-}$ and Lyz-TLR4$^{-/-}$ mice compared with wild-type mice on day 7, but not on day 28 (Fig. 1, *right*). No significant difference in bone healing based on micro–computed tomography was found between TLR4$^{-/-}$ and Lyz-TLR4$^{-/-}$ mice at any time point (Fig. 1, *right*).

To further demonstrate the accelerated healing response in TLR4$^{-/-}$ and Lyz-TLR4$^{-/-}$ mice, hematoxylin and eosin staining, pentachrome staining, and immunohistochemistry staining for osteopontin were performed. Histologic healing patterns at day 7 demonstrated larger areas of newly formed woven bone at the endocortical side of calvaria bone in TLR4$^{-/-}$ and Lyz-TLR4$^{-/-}$ mice compared with wild-type mice, accompanied by active osteoblast infiltration and enhanced osteopontin staining (Fig. 2, *left* and Fig. 3, *left*). Histomorphometric measurements showed significantly larger areas of newly formed bone and significantly more infiltrated osteoblasts in the TLR4$^{-/-}$ and Lyz-TLR4$^{-/-}$ mice compared with wild-type mice at day 7 (Fig. 2, *right* and Fig. 3, *right*). On day 28, similar histologic characteristics were seen among the three groups. Although woven bone matrix was still evident, mature lamellar bone was present on the ectocortical and endocortical calvarial sides in all groups on day 28. [**See Figure, Supplemental Digital Content 1,** which shows comparable bone formation among all groups on day 28. (*Left*) A similar histologic healing pattern was observed in all groups, and no groups showed complete bone healing at day 28. (*Right*) One-way analysis of variance

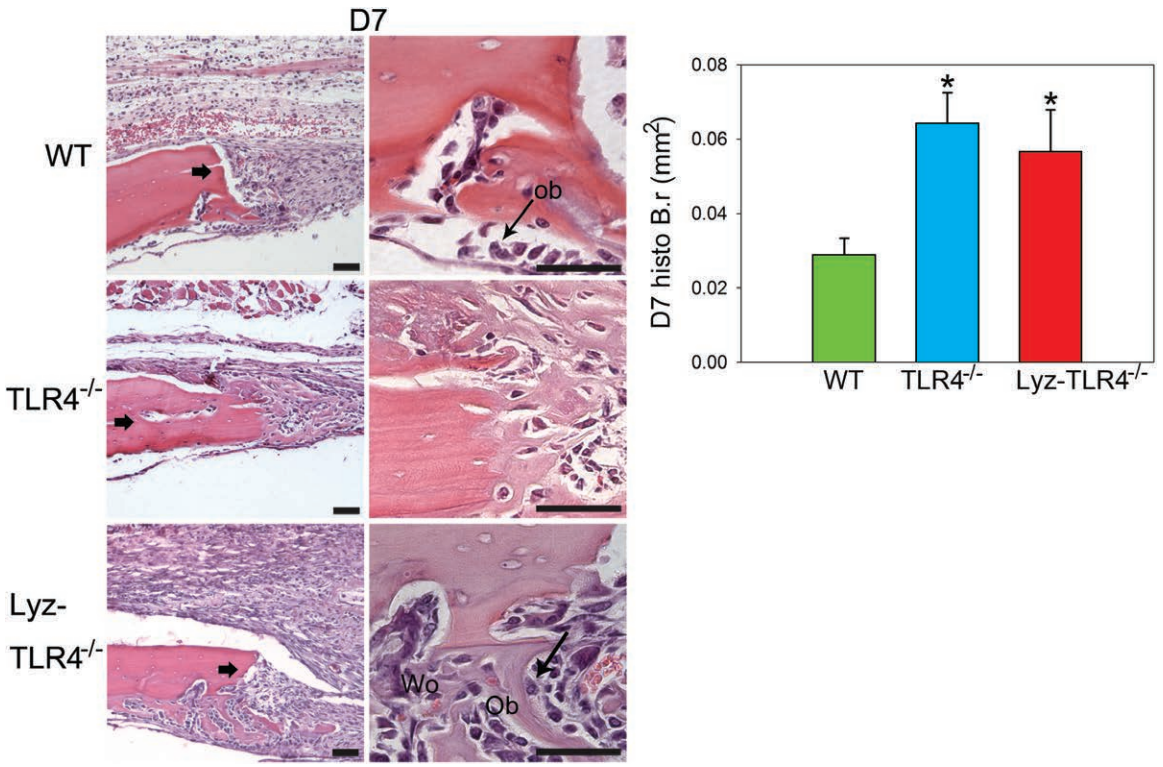

Fig. 2. Fast bone formation in TLR4$^{-/-}$ and Lyz-TLR4$^{-/-}$ mice. (*Left*) Representative hematoxylin and eosin–stained images at day 7. Disorganized loose connective tissue completely filled the bone defect on day 7 in all groups. Larger area of newly formed cellularized-woven bone was observed in TLR4$^{-/-}$ and Lyz-TLR4$^{-/-}$ mice compared with wild-type (*WT*) mice. (*Right*) One-way analysis of variance showed significantly large areas of bone formation in TLR4$^{-/-}$ and Lyz-TLR4$^{-/-}$ mice compared with wild-type mice at postoperative day 7 (n = 3 to 5 per group per time point, mean ± SEM; *scale bar* = 50 μm; *bold arrow*, defect margin; *Ob*, osteoblast; *Wo*, woven bone; *B.r*, bone area; $p < 0.05$, *versus wild-type).

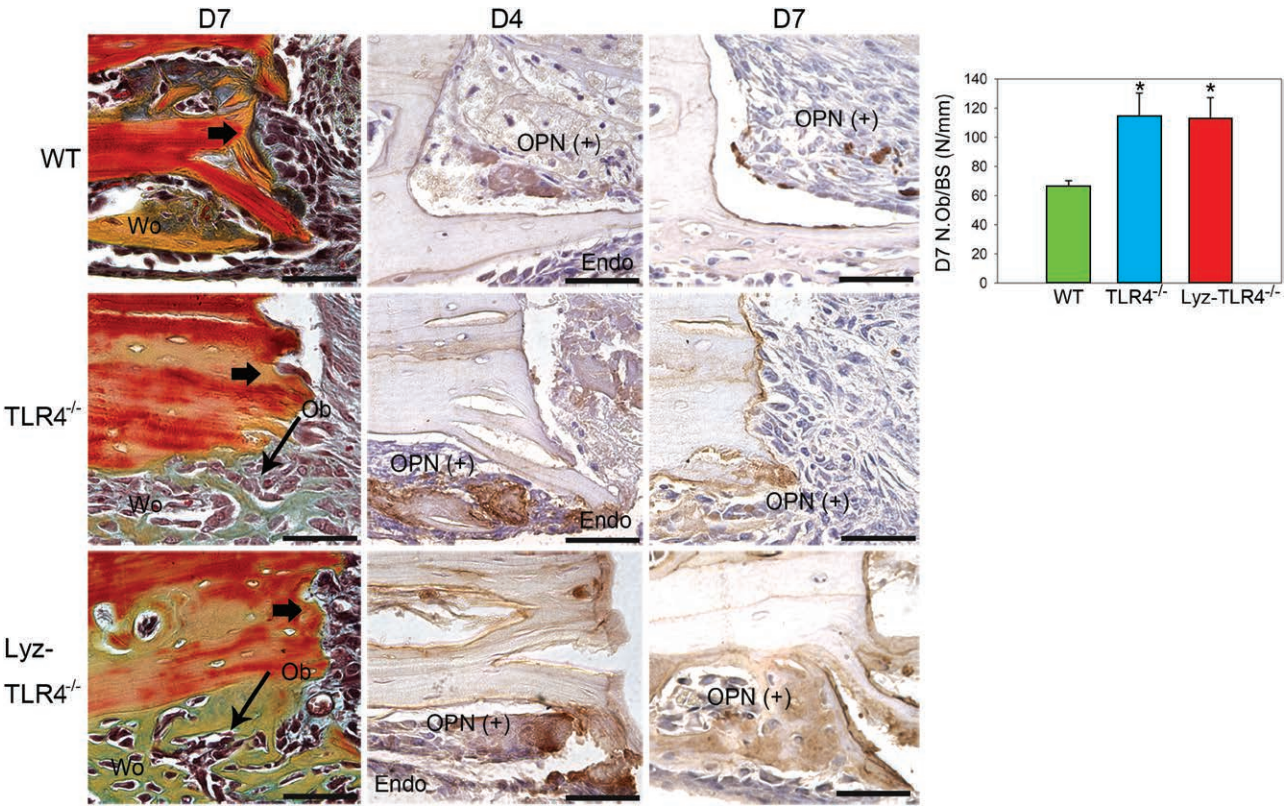

Fig. 3. Accelerated intramembranous bone formation in TLR4$^{-/-}$ and Lyz-TLR4$^{-/-}$ mice. (*Left*) Representative pentachrome-stained and anti–osteopontin-stained images. One or two layers of bone surface–lining osteoblasts were observed on the endocortical side of calvarial bone in wild-type (*WT*) mice. More infiltrated osteoblasts, larger areas of newly formed woven bone matrix (*yellow* in pentachrome staining), and more intense osteopontin staining were evident in both TLR4$^{-/-}$ and Lyz-TLR4$^{-/-}$ mice than in wild-type mice. (*Right*) One-way analysis of variance showed significantly more osteoblasts in TLR4$^{-/-}$ and Lyz-TLR4$^{-/-}$ mice compared with wild-type mice at postoperative day 7 (n = 3 to 5 per group per time point for histologic analyses, mean ± SEM; *scale bar* = 50 μm; *bold arrow*, defect margin; *Ob*, osteoblast; *Wo*, woven bone, *Endo*, endocortical side; $p < 0.05$, *versus wild-type).

showed that no significant difference was detected in bone formation among three groups on day 28 (n = 3 to 5 per group per time point, mean ± SEM; *scale bar* = 50 μm; *bold arrow*, defect margin; *WT*, wild-type; *Wo*, woven bone, *LB*, lamellar bone; *B.r*, bone area), ***http://links.lww.com/PRS/C264***.] No significant difference in new bone areas or osteoblast numbers was found between TLR4$^{-/-}$ and Lyz-TLR4$^{-/-}$ mice on day 7 (Fig. 2, *right* and Fig. 3, *right*) or between the three groups on day 28.

Osteoclastogenesis In Vivo and In Vitro

To gain better understanding of osteoclast infiltration and tissue resorption during the early phase of the fracture healing process, tartrate-resistant acid phosphatase staining of paraffin-embedded slides of wild-type, TLR4$^{-/-}$, and Lyz-TLR4$^{-/-}$ mice was performed on days 7 and 14. Tartrate-resistant acid phosphatase–positive osteoclasts were evident at the defect margin and newly regenerated woven bone in all groups at day 7 (Fig. 4, *left*). More intense tartrate-resistant acid phosphatase–positive staining and significantly more osteoclasts were detected in Lyz-TLR4$^{-/-}$ mice relative to wild-type mice at day 7 (Fig. 4). The number of osteoclasts did not differ significantly between TLR4$^{-/-}$ mice and Lyz-TLR4$^{-/-}$ mice at day 7 (Fig. 4, *right*). No significant difference in the number of osteoclasts was observed between the three groups at day 14 (Fig. 4, *right*).

To better understand the differentiation capacity and resorption activity of osteoclasts in wild-type, TLR4$^{-/-}$, and Lyz-TLR4$^{-/-}$ mice, in vitro differentiation and resorption assay were performed on harvested bone marrow–derived primary cells. At day-8 culture, more osteoclasts (red tartrate-resistant acid phosphatase–positive, multinucleated cells) were observed in the TLR4$^{-/-}$ and Lyz-TLR4$^{-/-}$ groups compared with the wild-type group (Fig. 5, *left*). Large areas of resorption pits were also seen in TLR4$^{-/-}$ and Lyz-TLR4$^{-/-}$ groups than in wild-type

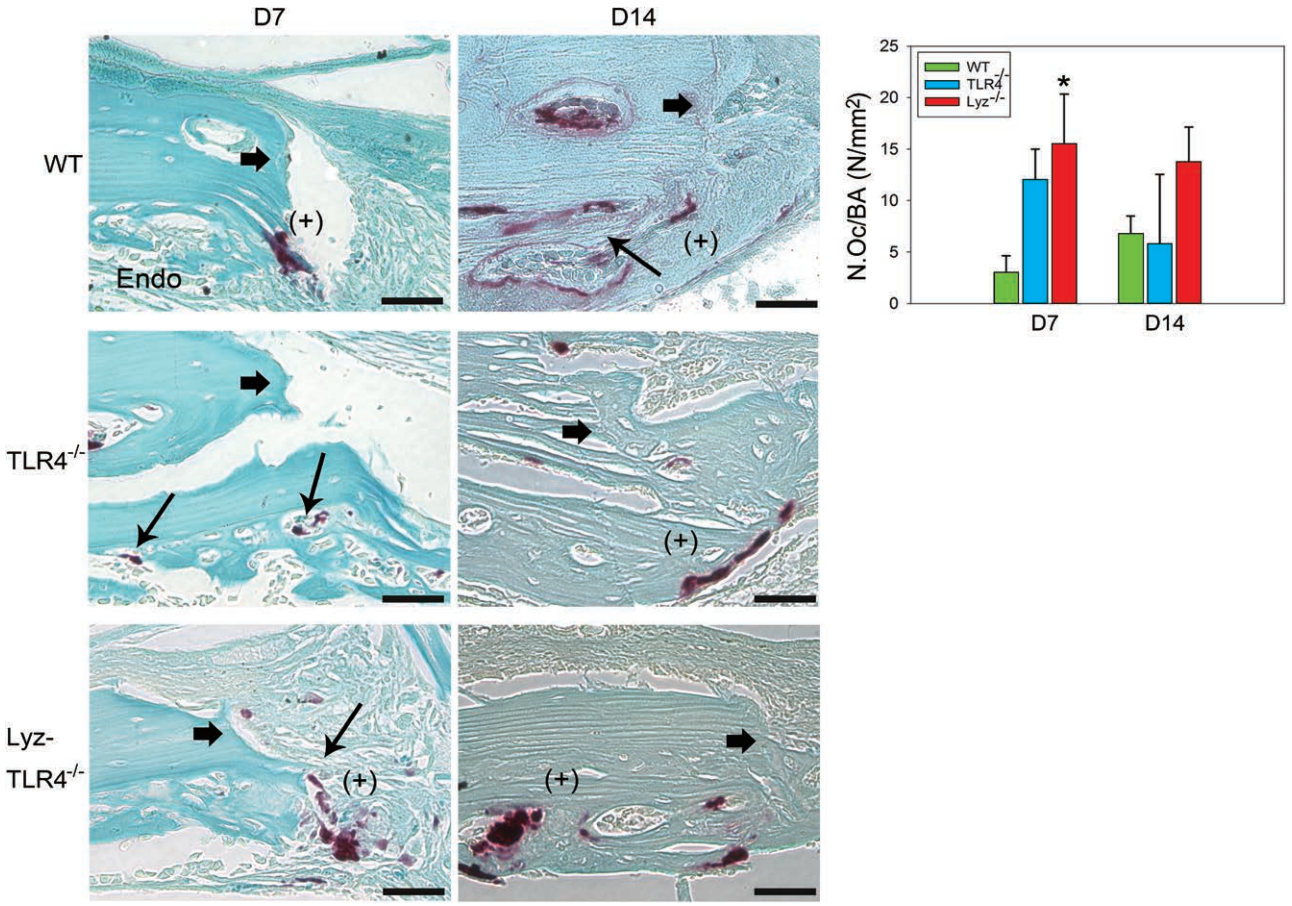

Fig. 4. Enhanced osteoclastogenesis in TLR4$^{-/-}$ and Lyz-TLR4$^{-/-}$ mice. (*Left*) Representative tartrate-resistant acid phosphatase–stained images at days 7 and 14. Tartrate-resistant acid phosphatase–positive osteoclasts were evident at the defect margin and the bone marrow space. At day 7, more intense tartrate-resistant acid phosphatase–positive staining was shown in Lyz-TLR4$^{-/-}$ mice compared with wild-type (*WT*) mice. This observation was consistent with the tartrate-resistant acid phosphatase–positive osteoclast counts shown (*right*). No significant difference in numbers of tartrate-resistant acid phosphatase–positive osteoclast was shown between TLR4$^{-/-}$ mice and Lyz-TLR4$^{-/-}$ mice at day 7 or between all three groups at day 14 (n = 3 to 5 per group per time point for histologic analyses, mean ± SEM; *scale bars* = 50 μm; *bold arrow*, defect margin, *Endo*, endocortical side; $p < 0.05$; *compared to wild-type mice).

group at day 8 (Fig. 5, *second from left*). Consistent with these observations, significantly larger osteoclast ratio (osteoclasts/total cells) and resorption areas were observed in the TLR4$^{-/-}$ and Lyz-TLR4$^{-/-}$ groups compared to the wild-type group on day 8 (Fig. 5, *second from right* and *right*). At day 11, no significant differences in osteoclast ratio (data not shown) or resorption areas were found among the three groups (Fig. 5, *second from left* and *right*).

Characterizing Macrophage Infiltration during Early Calvarial Bone Healing

To better understand macrophage infiltration during early fracture healing, anti-F4/80, anti-CD163, and anti-Arginase 1 immunohistochemistry staining were analyzed. At day 1, similar intense staining of anti-F4/80 indicating infiltration of M0 macrophages, anti-CD163 indicating M1 macrophages, and anti-Arginase1 staining indicating M2 macrophages were evident in all groups (Fig. 6). [**See Figure, Supplemental Digital Content 2,** which shows representative anti-CD163–stained images at day 1. Similar staining was observed in wild-type (*WT*), TLR4-/-, and Lyz-TLR4-/- mice at day 1. (n = 3 to 5 per group per time point; *scale bar* = 50 μm; *bold arrow*, defect margin; Endo, endocortical side), ***http://links.lww.com/PRS/C265***.] At days 4 and 7, no obvious anti-F4/80 or similar anti–Arginase1-positive staining was observed in any of the groups (data not shown).

DISCUSSION

The aim of this study was to investigate the effect of toll-like receptor 4 depletion on osteoclastogenesis and its impact on bone healing.

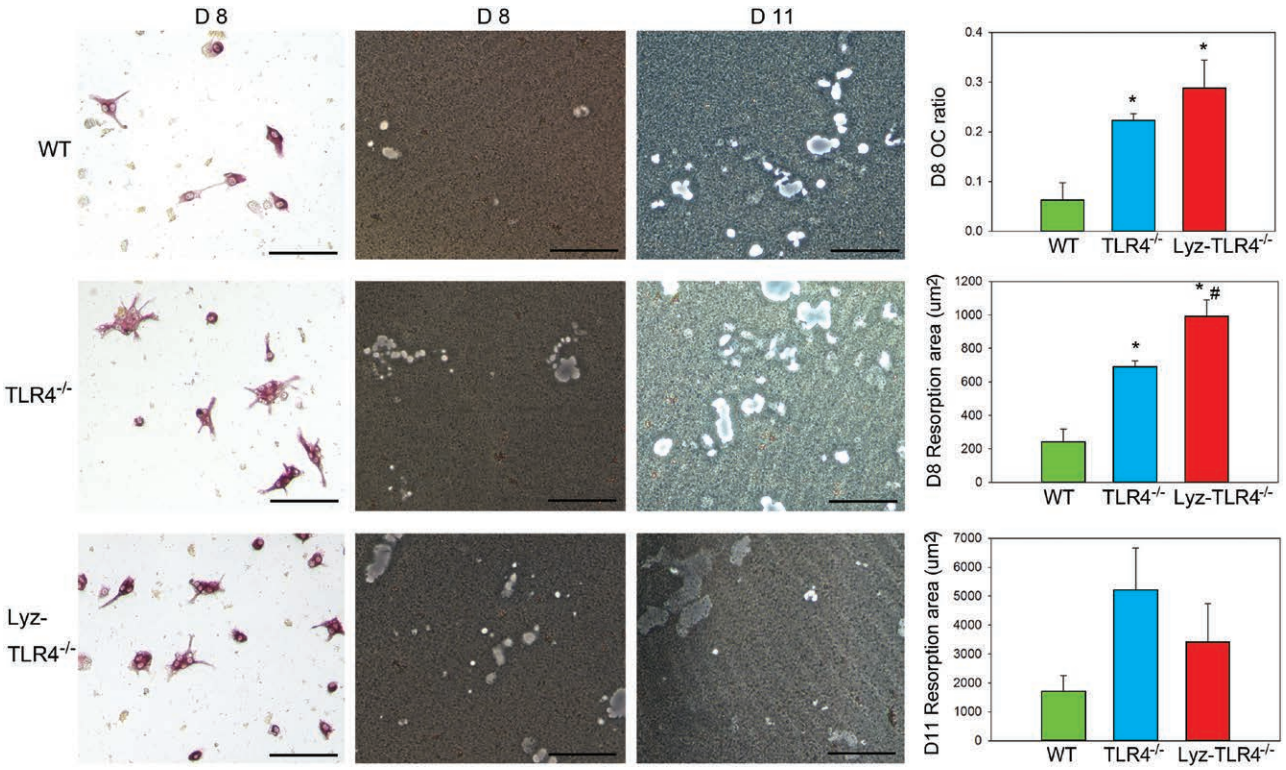

Fig. 5. In vitro osteoclast differentiation and resorption analyses at days 8 and 11. (*Left*) Representative tartrate-resistant acid phosphatase–stained images at day 8. More osteoclasts (tartrate-resistant acid phosphatase–positive multinucleated cells) were observed in TLR4$^{-/-}$ and Lyz-TLR4$^{-/-}$ mice compared with the wild-type (*WT*) group. This observation was consistent with osteoclast measurement results (numbers of osteoclasts over total cells) shown (*right, top*). (*Second from left* and *second from right*) Representative images of resorption pits at days 8 and 11. (*Right, middle*) Significantly larger areas of resorption pits were observed in TLR4$^{-/-}$ mice and Lyz-TLR4$^{-/-}$ mice compared with wild-type mice, and in Lyz-TLR4$^{-/-}$ mice compared with TLR4$^{-/-}$ mice at day 8. (*Right, bottom*) Comparable resorption areas were observed between the three groups at day 11 (n = 6 to 8 per group per time point, mean ± SEM; *scale bars* = 100 μm; $p < 0.05$, *versus wild-type mice, #versus TLR4$^{-/-}$ mice).

Consistent with our hypothesis, accelerated bone healing, increased infiltration of osteoclasts within a noncompromised calvarial defect model, and enhanced osteoclastogenesis and resorption activity from in vitro assay were observed in Lyz-TLR4$^{-/-}$ mice compared to wild-type mice, suggesting an important role of toll-like receptor 4 in regulating osteoclastogenic differentiation during fracture healing.

Previous studies showed that enhanced osteoclast activity is the main driving force for chronic inflammation-stimulated bone destruction[15,23]; however, in our noncompromised calvarial defect model, it initiates an earlier bone repair cascade. Collectively, our data, together with previous work linking toll-like receptor 4 with bone destruction in inflammatory disease,[23–25] suggest that toll-like receptor 4 may act as a "switch," directing precursors toward differentiation into either inflammatory cells or bone-resorbing osteoclasts. This regulatory role of toll-like receptor 4 in osteoclastogenesis might be because toll-like receptor 4 can signal through two adaptor proteins, MyD88 and TRIF. This unique property of toll-like receptor 4 has also been reported in other animal models. For example, toll-like receptor 4 signaling through the MyD88-dependent pathway contributes to ischemic brain damage,[26–28] whereas TRIF-mediated signaling exerts a neuroprotective effect against cerebral ischemia.[29] Thus, the functional consequences of toll-like receptor 4 activation on tissue regeneration might depend on its activation through different signaling pathways. In addition, studies have also suggested that toll-like receptor activation in osteoclast precursors maintains their phagocytic activity and inhibits their differentiation into noninflammatory mature osteoclasts, whereas toll-like receptor activation on mature osteoclasts increases their survival rate.[14] In light of these findings, toll-like receptor 4 may be involved in regulating the balance between immune response and bone metabolism

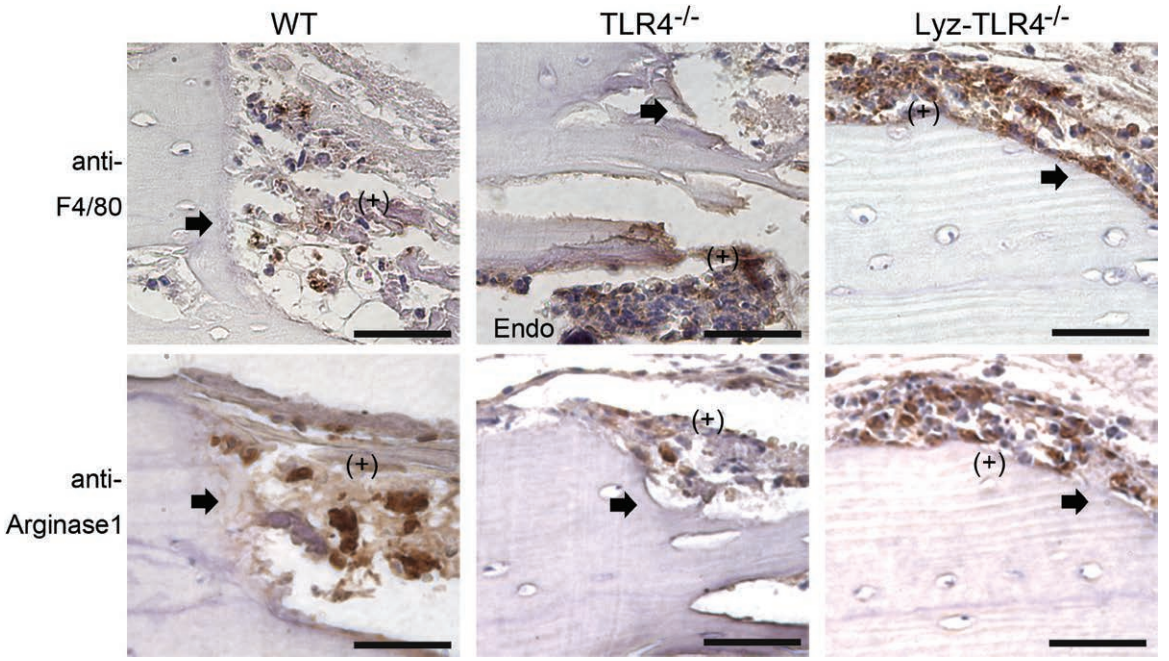

Fig. 6. Macrophage infiltration during early fracture healing. Representative anti-F4/80– and anti-Arginase1–stained images at day 1. Similar anti-F4/80 staining and anti-Arginase1 staining, suggesting comparable M0 and M2 macrophage infiltration, was observed in wild-type (*WT*), TLR4$^{-/-}$, and Lyz-TLR4$^{-/-}$ mice at day 1 (n = 3 to 5 per group per time point for histology analyses; *scale bar* = 50 μm; *bold arrow*, defect margin; *Endo*, endocortical side).

at different stages of differentiation by using different downstream pathways.

Macrophages are highly involved in regulating inflammation, and also play an integral role in tissue regeneration. Within the first 3 days of injury, macrophages infiltrate into the wound bed, participating in the inflammatory response and débridement process by means of phagocytosis activity and reactive radical release.[30] Lee et al. showed that macrophage activation and polarization influence kidney injury and repair.[31] Their data suggest that infusion of interferon-γ–stimulated, proinflammatory macrophages further exacerbated kidney-damaged mice, whereas infusion of M2 phenotype macrophages was correlated with kidney proliferation and repair.[31] As myeloid cells are also precursors for macrophages, depletion of toll-like receptor 4 in myeloid cells might also influence macrophage differentiation and polarization during bone repair. In our study, we observed similar infiltration levels of M0, M1, and M2 macrophages in wild-type, TLR4$^{-/-}$, and Lyz-TLR4$^{-/-}$ mice at day 1. Together, depletion of toll-like receptor 4 expression in myeloid cells did not seem to change macrophage-lineage differentiation or macrophage polarization in this calvarial defect model. However, more evidence is needed to gain a better understanding of the impact of toll-like receptor 4 depletion in myeloid cells on macrophage differentiation, phagocytic activity, and related inflammatory reaction.

This study is limited in that Cre combinase linked to Lyz is highly expressed in all myeloid-derived cells, including neutrophils, Kupffer cells, and monocytes, and as such, Lyz deletion of toll-like receptor 4 occurs in a range of myeloid-derived cells.[32] Thus, the mouse model is not above reproach, as it may provide a portion of cells that are not osteoclast progenitor specific in this study. Although there exist other animal models that target osteoclasts more specifically (e.g., cathepsin K or tartrate-resistant acid phosphatase promotors, which are expressed in mature osteoclasts or osteoclast precursors and osteoclasts, respectively),[33] these mouse models were not sufficient for our aims considered in this study. We aimed to test the effect of toll-like receptor 4 deletion on both osteoclastogenesis and macrophage polarization, because toll-like receptor 4 has been reported to have a profound role in mediating innate immune response and skeletal tissue homeostasis,[14–16] Thus, we used a calvarial defect model of myeloid lineage-specific TLR4$^{-/-}$ mice (Lyz-TLR4$^{-/-}$ mice), in which Cre under lysozyme promoter enables inducible recombinase expression in both osteoclast and macrophage precursors, to test the early development and differentiation of osteoclasts/macrophages after calvarial fracture.

Our data suggest that toll-like receptor 4 depletion in myeloid cells led to a similar phenotype (accelerated bone healing in a noncompromised calvarial defect model) compared to global TLR4$^{-/-}$ mice. Considered together with other studies that explored the link between toll-like receptor 4 and bone destruction in inflammatory disease,[14–16] this study suggests that toll-like receptor 4 signaling plays an important regulatory role in promoting bone destruction and initiating early bone healing, through controlling osteoclastogenesis in different settings. This highlights a potential opportunity in which appropriate modulation of the toll-like receptor 4 signaling pathway can be used to reduce bone destruction in inflammatory bone diseases or enhance early healing in bone defects to improve clinical outcomes.

Gregory M. Cooper, Ph.D.
B3F3, 3533 Rangos Research Building
530 45th Street
Pittsburgh, Pa. 15201
greg.cooper@chp.edu

ACKNOWLEDGMENTS

The authors are grateful to Adam Kubala for assistance in animal surgery, Thomas Prindle (The Johns Hopkins University) for assistance in knockout animal cloning and breeding, and Dai Fei Elmer Ker (Stanford University) for assistance in editing the article. The authors are especially grateful for National Science Foundation for Young Scientists of China grant no. 81201410 (to D.W., principal investigator) for supporting this study.

REFERENCES

1. Thomas MV, Puleo DA. Infection, inflammation, and bone regeneration: A paradoxical relationship. *J Dent Res.* 2011;90:1052–1061.
2. Eming SA, Hammerschmidt M, Krieg T, Roers A. Interrelation of immunity and tissue repair or regeneration. *Semin Cell Dev Biol.* 2009;20:517–527.
3. Alnaeeli M, Park J, Mahamed D, Penninger JM, Teng YT. Dendritic cells at the osteo-immune interface: Implications for inflammation-induced bone loss. *J Bone Miner Res.* 2007;22:775–780.
4. Mountziaris PM, Spicer PP, Kasper FK, Mikos AG. Harnessing and modulating inflammation in strategies for bone regeneration. *Tissue Eng Part B Rev.* 2011;17:393–402.
5. Rakoff-Nahoum S, Medzhitov R. Toll-like receptors and cancer. *Nat Rev Cancer* 2009;9:57–63.
6. Huebener P, Schwabe RF. Regulation of wound healing and organ fibrosis by toll-like receptors. *Biochim Biophys Acta* 2013;1832:1005–1017.
7. Lin Q, Li M, Fang D, Fang J, Su SB. The essential roles of Toll-like receptor signaling pathways in sterile inflammatory diseases. *Int Immunopharmacol.* 2011;11:1422–1432.
8. Nijland R, Hofland T, van Strijp JA. Recognition of LPS by TLR4: Potential for anti-inflammatory therapies. *Mar Drugs* 2014;12:4260–4273.
9. Smiley ST, King JA, Hancock WW. Fibrinogen stimulates macrophage chemokine secretion through toll-like receptor 4. *J Immunol.* 2001;167:2887–2894.
10. Gondokaryono SP, Ushio H, Niyonsaba F, et al. The extra domain A of fibronectin stimulates murine mast cells via toll-like receptor 4. *J Leukoc Biol.* 2007;82:657–665.
11. Ohashi K, Burkart V, Flohé S, Kolb H. Cutting edge: Heat shock protein 60 is a putative endogenous ligand of the toll-like receptor-4 complex. *J Immunol.* 2000;164:558–561.
12. Biragyn A, Ruffini PA, Leifer CA, et al. Toll-like receptor 4-dependent activation of dendritic cells by beta-defensin 2. *Science* 2002;298:1025–1029.
13. Yang H, Antoine DJ, Andersson U, Tracey KJ. The many faces of HMGB1: molecular structure-functional activity in inflammation, apoptosis, and chemotaxis. *J Leukoc Biol.* 2013;93:865–873.
14. Bar-Shavit Z. Taking a toll on the bones: Regulation of bone metabolism by innate immune regulators. *Autoimmunity* 2008;41:195–203.
15. Gómez R, Villalvilla A, Largo R, Gualillo O, Herrero-Beaumont G. TLR4 signalling in osteoarthritis: Finding targets for candidate DMOADs. *Nat Rev Rheumatol.* 2015;11:159–170.
16. Tomofuji T, Ekuni D, Azuma T, et al. Involvement of toll-like receptor 2 and 4 in association between dyslipidemia and osteoclast differentiation in apolipoprotein E deficient rat periodontium. *Lipids Health Dis.* 2013;12:1.
17. Ding YS, Zhao Y, Xiao YY, Zhao G. Toll-like receptor 4 gene polymorphism is associated with chronic periodontitis. *Int J Clin Exp Med.* 2015;8:6186–6192.
18. Uzar I, Mrozikiewicz PM, Bogacz A, et al. The importance of 8993C>T (Thr399Ile) TLR4 polymorphism in etiology of osteoporosis in postmenopausal women. *Ginekol Pol.* 2014;85:180–184.
19. Wang D, Gilbert JR, Cray JJ Jr, et al. Accelerated calvarial healing in mice lacking Toll-like receptor 4. *PLoS One* 2012;7:e46945.
20. Sodhi CP, Neal MD, Siggers R, et al. Intestinal epithelial Toll-like receptor 4 regulates goblet cell development and is required for necrotizing enterocolitis in mice. *Gastroenterology* 2012;143:708–718.e1.
21. Nace GW, Huang H, Klune JR, et al. Cellular-specific role of toll-like receptor 4 in hepatic ischemia-reperfusion injury in mice. *Hepatology* 2013;58:374–387.
22. Wang D, Gilbert JR, Shaw MA, et al. Toll-like receptor 4 mediates the regenerative effects of bone grafts for calvarial bone repair. *Tissue Eng Part A* 2015;21:1299–1308.
23. Vijayan V, Khandelwal M, Manglani K, Gupta S, Surolia A. Methionine down-regulates TLR4/MyD88/NF-κB signalling in osteoclast precursors to reduce bone loss during osteoporosis. *Br J Pharmacol.* 2014;171:107–121.
24. Huang RL, Yuan Y, Zou GM, Liu G, Tu J, Li Q. LPS-stimulated inflammatory environment inhibits BMP-2-induced osteoblastic differentiation through crosstalk between TLR4/MyD88/NF-κB and BMP/Smad signaling. *Stem Cells Dev.* 2014;23:277–289.
25. Kikuchi T, Matsuguchi T, Tsuboi N, et al. Gene expression of osteoclast differentiation factor is induced by lipopolysaccharide in mouse osteoblasts via Toll-like receptors. *J Immunol.* 2001;166:3574–3579.
26. Yang QW, Lu FL, Zhou Y, et al. HMBG1 mediates ischemia-reperfusion injury by TRIF-adaptor independent Toll-like receptor 4 signaling. *J Cereb Blood Flow Metab.* 2011;31:593–605.
27. Gao Y, Fang X, Sun H, et al. Toll-like receptor 4-mediated myeloid differentiation factor 88-dependent signaling pathway

is activated by cerebral ischemia-reperfusion in hippocampal CA1 region in mice. *Biol Pharm Bull.* 2009;32:1665–1671.
28. Hyakkoku K, Hamanaka J, Tsuruma K, et al. Toll-like receptor 4 (TLR4), but not TLR3 or TLR9, knock-out mice have neuroprotective effects against focal cerebral ischemia. *Neuroscience* 2010;171:258–267.
29. Vartanian KB, Stevens SL, Marsh BJ, Williams-Karnesky R, Lessov NS, Stenzel-Poore MP. LPS preconditioning redirects TLR signaling following stroke: TRIF-IRF3 plays a seminal role in mediating tolerance to ischemic injury. *J Neuroinflammation.* 2011;8:140.
30. Geissmann F, Manz MG, Jung S, Sieweke MH, Merad M, Ley K. Development of monocytes, macrophages, and dendritic cells. *Science* 2010;327:656–661.
31. Lee S, Huen S, Nishio H, et al. Distinct macrophage phenotypes contribute to kidney injury and repair. *J Am Soc Nephrol.* 2011;22:317–326.
32. Hilliard TJ, Meadows G, Kahn AJ. Lysozyme synthesis in osteoclasts. *J Bone Miner Res.* 1990;5:1217–1222.
33. Chiu WS, McManus JF, Notini AJ, Cassady AI, Zajac JD, Davey RA. Transgenic mice that express Cre recombinase in osteoclasts. *Genesis* 2004;39:178–185.